ESR measurements of phosphorus dimers in isotopically enriched ^{28}Si silicon

S. Shankar,* A. M. Tyryshkin, and S. A. Lyon

Dept. of Electrical Engineering, Princeton University, Princeton, NJ 08544, USA

(Dated: July 20, 2018)

Abstract

Dopants in silicon have been studied for many decades using optical and electron spin resonance (ESR) spectroscopy. Recently, new features have been observed in the spectra of dopants in isotopically enriched ^{28}Si since the reduced inhomogeneous linewidth in this material improves spectral resolution. With this in mind, we measured ESR on exchange coupled phosphorus dimers in ^{28}Si and report two results. First, a new fine structure is observed in the ESR spectrum arising from state mixing by the hyperfine coupling to the ^{31}P nuclei, which is enhanced when the exchange energy is comparable to the Zeeman energy. This fine structure enables us to spectroscopically address two separate dimer sub-ensembles, the first with exchange (J) coupling ranging from 2 to 7 GHz and the second with J ranging from 6 to 60 GHz. Next, the average spin relaxation times, T_1 and T_2 of both dimer sub-ensembles were measured using pulsed ESR at 0.35 T. Both T_1 and T_2 for transitions between triplet states of the dimers were found to be identical to the relaxation times of isolated phosphorus donors in ^{28}Si, with $T_2 = 4\,\mathrm{ms}$ at $1.7\,\mathrm{K}$ limited by spectral diffusion due to dipolar interactions with neighboring donor electron spins. This result, consistent with theoretical predictions, implies that an exchange coupling of 2–60 GHz does not limit the dimer T_1 and T_2 in bulk Si at the 10 ms timescale.

PACS numbers: 76.30.-v, 71.55.Cn

* shyam.shankar@yale.edu; Now at Department of Applied Physics, Yale University, New Haven, CT 06511.

I. INTRODUCTION

Natural silicon contains three stable isotopes: 92.2 % of ^{28}Si, 4.7 % of ^{29}Si, and 3.1 % of ^{30}Si. A concerted effort has been made over the last decade to grow isotopically enriched silicon crystals, with 99.9 % and higher content of only one isotope[1–3], for use in a variety of fields such as metrology[4] and quantum computing[5]. The availability of such isotopically enriched silicon is of great interest for spectroscopy since it can significantly reduce inhomogeneous spectral linewidths and therefore improve spectral resolution. For example, two recent reports have resolved new fine structures in the optical spectra of phosphorus donors[6] and in the electron spin resonance (ESR) spectra of boron acceptors[7] in ^{28}Si. These fine spectral structures were unresolvable in natural silicon because of the inhomogeneous broadening arising from the presence of magnetic ^{29}Si nuclei. Furthermore, the absence of ^{29}Si nuclei in isotopically enriched ^{28}Si silicon, eliminates the spectral diffusion decoherence mechanism for donors in silicon[8], an otherwise dominant source of decoherence in solid-state spin-based quantum computing architectures[9, 10]. In this paper, we perform ESR of exchange coupled phosphorus dimers in isotopically purified ^{28}Si. The improved spectral resolution arising from isotopic enrichment enables us to observe a previously unresolved fine structure in the dimer ESR line. We then perform pulsed ESR experiments and place limits on the decoherence of phosphorus dimers arising from the presence of exchange coupling.

Dopants in natural silicon have been studied for over fifty years by ESR spectroscopy[11]. A typical continuous wave (CW) ESR spectrum of phosphorus donors in natural silicon is shown in Fig. 1(a). The spectral lines are inhomogeneously broadened by hyperfine interactions with the 4.7 % of ^{29}Si (nuclear spin $I = 1/2$)[11, 12]. On the other hand, the spectrum measured in isotopically enriched ^{28}Si, also shown in Fig. 1(a), demonstrates a reduced spectral linewidth (the ^{28}Si nucleus has no magnetic moment, $I = 0$). In moderately doped samples ($\sim 10^{16}\,\mathrm{cm}^{-3}$), a weak line is also observed at the center of the donor doublet that arises from pairs of donors that are close enough to form exchange (J) coupled dimers[13, 14]. Since the crystals are randomly doped, the dimers are present with a broad range of distances between dopants and therefore a broad distribution of J couplings. The central ESR line arises from a subset of dimers with J greater than the hyperfine coupling ($A = 117\,\mathrm{MHz} \equiv 4.2\,\mathrm{mT}$) to the donor ^{31}P nucleus[15]. In Fig. 1(b), we show that the reduced

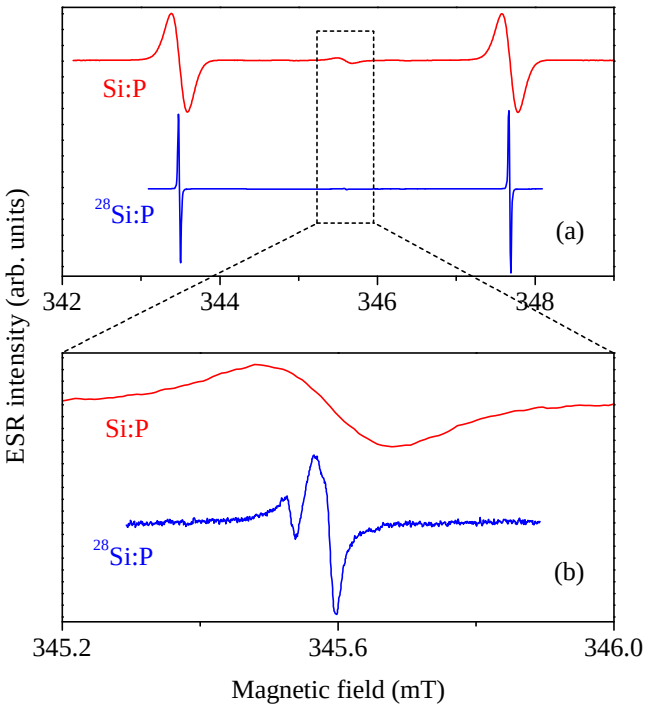

FIG. 1. (a) ESR spectra from phosphorus dopants in natural silicon (Si:P) and isotopically enriched ^{28}Si (^{28}Si:P), measured at 15 K. Phosphorus doping densities were $\sim 2 \times 10^{16}$ cm^{-3} (see other details of the samples in the text). Two strong lines split by 4.2 mT are from isolated donors. Weak line in the center is from donor dimers. Two outer lines from the dimers overlap with the stronger lines from isolated donors and are therefore unobservable. (b) Zoom in to the center region showing details of the central line from dimers.

linewidth in ^{28}Si allows us to observe a new fine structure in the dimer ESR line with a splitting of about 60 µT. Since J is greater than A, the eigenstates of the dimer consist of a spin-0 singlet (S) and three spin-1 triplet states (T_+, T_0, T_-) and our ESR experiment probes transitions among the three triplet states. Below, we will explain through simulations that this new fine structure is a result of the second order mixing between the S and T_0 states. This mixing arises from an interplay between the ^{31}P hyperfine, exchange and Zeeman energies, with the mixing being strongest when the exchange coupling is approximately equal to the Zeeman energy. Further, we will show that this mixing allows the use of ESR transitions between the triplet states to probe spin relaxation between the S and T_0 triplet state, even though the S state is ESR-silent in our experiments.

We performed pulsed ESR to measure spin relaxation times T_1 and T_2 of dimers, in order to examine whether the presence of exchange coupling within the dimer gives rise to decoherence in excess of that for the isolated donor. The exchange interaction between two phosphorus donors is the canonical method to implement a two-qubit gate [5, 10, 16], and therefore any additional decoherence arising from exchange would be of critical importance for donor-based quantum computing schemes. Such decoherence can be caused by charge noise modulating the J-coupling, which would be an especially significant issue for donors near an interface and next to the control gates[17]. Furthermore, the S–T_0 state mixing arising from J-coupling opens an additional relaxation (T_1) pathway through the electron-phonon interaction[18]. These mechanisms could thus limit the usability of exchange to perform multi-qubit operations. In our experiments, the ability to resolve a fine structure in the dimer ESR line enables us to separately address two dimer sub-ensembles, the first with J ranging from 6 to 60 GHz and the second with J ranging from 2 to 7 GHz. We find that the relaxation times of these two dimer sub-ensembles are identical to that of isolated donors, thus limited by the same mechanism, namely spectral diffusion due to dipolar interactions with flip-flopping neighboring donors[19]. Thus, we find that the presence of J-coupling of 2–60 GHz in dimers does not introduce any additional decoherence in bulk Si on a timescale of 10 ms.

An ESR experiment directly probes the spin-dynamics among the triplet (T) states of the dimer. However, high-fidelity two-qubit gates require maintaining the coherence between all four spin states including the S state. Although our ESR experiments do not allow any direct information about the ESR-silent S state, nevertheless some important estimates can be made from T_2 times measured for T states. Specifically, the one-phonon T_1 process from T_0 to S, arising from the J-induced mixing[18], can result in an irreversible leakage of coherence from the triplet state during Hahn echo experiments. This would potentially result in faster T_2 decay times, which we do not see in our experiment. Our measured $T_2 = 4$ ms for triplet states thus implies that T_{S-T0} must be slower than 10 ms. This lower bound, consistent with recent theoretical calculations[18] and experimental results[20], is encouraging for spin-based quantum computing schemes since it suggests that the presence of exchange coupling does not cause any additional relaxation between the triplet and singlet states at the level of about 10 ms in a bulk crystal.

Finally, while measuring T_2 using a standard Hahn echo experiment[21], we observed an

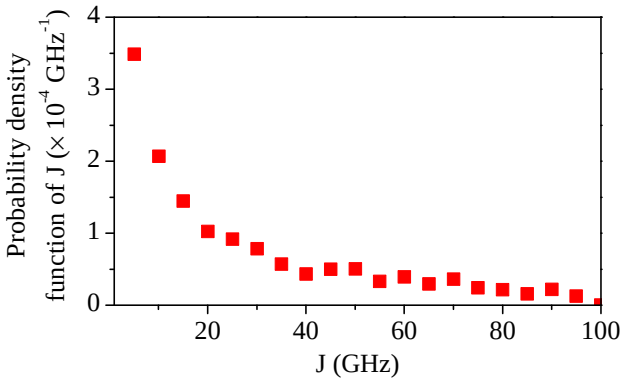

FIG. 2. Distribution function of dimer J couplings calculated for a doping density $2 \times 10^{16}\,\mathrm{cm}^{-3}$. Only high J range between 1 GHz and 100 GHz is shown specific to dimers selectively observed in our experiments. The complete distribution function, including the low J range, is shown in Fig. 9 in the Appendix.

unusual dependence of the echo decay on pulse lengths and powers. Through numerical simulations we explain that this dependence arises from electron spin echo envelope modulation (ESEEM) effects in high-spin dimers[22] and destructive interference of the ESEEM from different dimers due to a broad J-coupling distribution in the ensemble. These ESEEM effects, while creating additional difficulties in our experiments, can be viewed as a spectroscopic signature of J-coupled dimers and as such can be useful in studying donor dimers and also other coupled dimers.

II. EXPERIMENT

ESR experiments were performed using isotopically enriched ^{28}Si epi-layer wafers (99.9 % of ^{28}Si and 800 ppm of ^{29}Si) doped with phosphorus to a density of $1.6 \times 10^{16}\,\mathrm{cm}^{-3}$[3]. For comparison, we also measured a natural silicon crystal doped with phosphorus to a density of $1.7 \times 10^{16}\,\mathrm{cm}^{-3}$. These samples were previously used in our pulsed ESR study of isolated donors at temperatures down to 7 K in Ref. 8, where these samples were labeled as "^{28}Si:P-10^{16}" and "Si:P-10^{16}", respectively. The CW ESR spectra shown in Fig. 1 were measured using these silicon samples.

The random distribution of dopants in silicon implies that dimers are present with a broad range of J couplings[15]. We modified previously used methods to calculate the distribution

of J for our dopant density of about $2 \times 10^{16}\,\mathrm{cm}^{-3}$. Details of this calculation are presented in the Appendix where we compare our result with the previous results in Ref. 15. Only a small fraction of the donor pairs that have J greater than the ^{31}P hyperfine coupling of 117 MHz contribute to the central dimer line in the ESR experiment[14]. In Fig. 2, we show the calculated probability density function for J of those dimers that we selectively observe in our experiments. Our pulsed ESR experiments are sensitive to an even narrower range of J. As discussed below, a majority of our pulsed experiments were performed on the high-field component of the dimer fine structure, centered at 345.63 mT. In this case about 90% of the measured signal arises from a sub-ensemble of dimers with J ranging from about 6 to 60 GHz. We also performed an experiment 60 µT below, on the low-field component of the fine structure, for which most of the signal arises from a dimer sub-ensemble with J ranging from about 2 to 7 GHz.

CW and pulsed ESR measurements were performed at X-band (9.66 GHz) with a Bruker Elexsys 580 ESR spectrometer in a Bruker MD-5 dielectric resonator. An Oxford CF935 helium flow cryostat was used to maintain temperatures down to 5 K, while a temperature of 1.7 K was achieved by filling the cryostat with liquid helium and pumping. As T_1 was found to be exponentially dependent on temperature, the sample temperature was precisely controlled to within 0.1 K using an Oxford ITC503 temperature controller.

T_1 and T_2 were measured using the standard inversion recovery and Hahn echo pulse sequences[23]. In the inversion recovery sequence ($\pi - t - \pi/2 - \tau - \pi - \tau -$ echo), the echo intensity was measured as a function of delay, t, after the initial inverting π pulse. The measured intensity was fit by an exponential dependence to give the characteristic time T_1. Similarly, in the 2-pulse Hahn echo sequence ($\pi/2 - \tau - \pi - \tau -$ echo), the echo intensity measured as a function of total time 2τ was fit with an exponential decay to give the characteristic time T_2. In all pulsed experiments, the echo signal intensity was integrated using a 800 ns window symmetrically positioned on top of the echo signal. This integration corresponds to applying a detection bandwidth of 1.2 MHz (40 µT), i.e. only those dimers which have their resonance field within ±20 µT of the applied magnetic field were detected. Finally, a 16-step phase cycling sequence was used to remove any extraneous signals arising from microwave pulse imperfections (e.g., free induction decay signals) that could contaminate the echo decays. In order to eliminate contributions from broad background signals, the echo decays were also measured at a field 0.5 mT higher than

the dimer line and the resulting background decay was subtracted from the dimer decays before fitting to extract the relaxation times.

In order to compare the dimer T_2 with those of isolated donors, we also measured T_2 for isolated donors in the ^{28}Si sample at temperatures down to 1.7 K, thus extending the results of Ref. 8 to lower temperature. As in Ref. 8, the effect of instantaneous diffusion[24] on the T_2 relaxation of isolated donors was removed by performing a series of 2-pulse experiments ($\pi/2$ – τ – θ_2 – τ – echo) with reduced rotation angle (θ_2) for the second pulse, and extrapolating the measured T_2's to that which would be measured if θ_2 was zero. This extrapolated T_2 then measures the T_2 for isolated donors without instantaneous diffusion.

III. RESULTS

In the following sections we describe our experimental results and provide their interpretation. The new fine structure resolved in the dimer ESR signal in ^{28}Si is described in Sec. III A. The T_1 and T_2 results are discussed in Sec. III B. While measuring the Hahn echo from dimers, we found an unusual dependence of the echo decay on the pulse lengths and powers. This behavior is explained through ESEEM simulations in Sec. III C.

A. Fine structure in the dimer ESR lineshape

The full spin Hamiltonian for a dimer in a magnetic field, B_0, directed along the z-axis, expressed in frequency units[15] is

$$\begin{aligned}\mathcal{H} =&\nu_e(S_{1z}+S_{2z}) + J(\boldsymbol{S_1}\cdot\boldsymbol{S_2}) + A(\boldsymbol{S_1}\cdot\boldsymbol{I_1}+\boldsymbol{S_2}\cdot\boldsymbol{I_2}) + \\ &+\nu_n(I_{1z}+I_{2z}).\end{aligned} \tag{1}$$

In this equation, $\boldsymbol{S_i}$ and $\boldsymbol{I_i}$ are the electron and nuclear spins of two donors ($i = 1, 2$) forming a dimer ($I = S = 1/2$ for phosphorus donors); $\nu_e = g\mu_B B_0$ is the electron Larmor frequency (~ 9.66 GHz), with $g = 1.9985$ being the electron g-factor, and μ_B the Bohr magneton; J is the exchange coupling between donors; A is the ^{31}P hyperfine coupling (~ 117 MHz); and ν_n is the nuclear Larmor frequency (~ 6 MHz).

In the product basis $\mid S_{1z}S_{2z}I_{1z}I_{2z}\rangle$, the hyperfine coupling term can be split into a

TABLE I. Approximate eigenstates and eigenvalues of the dimer spin Hamiltonian (Eqn. 1), ignoring the off-diagonal terms resulting from the hyperfine coupling (Eqn. 2).

Eigenstates	Eigenvalues
$\mid T_+, t_+\rangle$	$\nu_e + J/4 + A/2 + \nu_n$
$\mid T_+, t_0\rangle, \mid T_+, s\rangle$	$\nu_e + J/4$
$\mid T_+, t_-\rangle$	$\nu_e + J/4 - A/2 - \nu_n$
$\mid T_0, t_+\rangle$	$J/4 + \nu_n$
$\mid T_0, t_0\rangle, \mid T_0, s\rangle$	$-J/4 + 1/2\sqrt{J^2 + A^2}$
$\mid T_0, t_-\rangle$	$J/4 - \nu_n$
$\mid T_-, t_+\rangle$	$-\nu_e + J/4 - A/2 + \nu_n$
$\mid T_-, t_0\rangle, \mid T_-, s\rangle$	$-\nu_e + J/4$
$\mid T_-, t_-\rangle$	$-\nu_e + J/4 + A/2 - \nu_n$
$\mid S, t_+\rangle$	$-3J/4 + \nu_n$
$\mid S, t_0\rangle, \mid S, s\rangle$	$-J/4 - 1/2\sqrt{J^2 + A^2}$
$\mid S, t_-\rangle$	$-3J/4 - \nu_n$

diagonal part $A(S_{1z}I_{1z} + S_{2z}I_{2z})$ and an off-diagonal part

$$\mathcal{H}_{off} = A/2(S_{1+}I_{1-} + S_{1-}I_{1+} + S_{2+}I_{2-} + S_{2-}I_{2+}). \tag{2}$$

Assuming $|\nu_e - J| \gg A$ (i.e. J far away from ν_e), the off-diagonal part of the hyperfine coupling can be neglected, and $\mathcal{H}$ can be diagonalized analytically[15]. The eigenstates and eigenvalues corresponding to this case are displayed in Table I, where uppercase letters (S, T_+, T_0, T_-) denote the electron singlet and triplet states, while lowercase letters (s, t_+, t_0, t_-) denote the nuclear singlet and triplet states. Including the off-diagonal terms (Eqn. 2) results in additional mixing of the eigenstates and second-order shifts to the eigenvalues of order $A^2/|\nu_e \pm J|$ or A^2/J[18].

In an ESR experiment, the only transitions excited are those that flip the electron state

($\Delta M_S = \pm 1$) while preserving the nuclear state ($\Delta M_I = 0$). Therefore, eight ESR transitions are allowed between the twelve levels in Table I. These allowed transitions can be further combined into four pairs of transitions which have identical transition frequencies. Two pairs, $\mid T_\pm, t_+\rangle \leftrightarrow \mid T_0, t_+\rangle$ and $\mid T_\pm, t_-\rangle \leftrightarrow \mid T_0, t_-\rangle$, with the nuclear spins in $\mid t_+\rangle$ and $\mid t_-\rangle$ states, respectively, have their transition frequencies coinciding with the transition frequencies of isolated donors; these transitions are unobservable in our experiments because they overlap with the much stronger transitions from isolated donors (e.g. the two intense lines in Fig. 1(a)). On the other hand, two other pairs, $\mid T_\pm, s\rangle \leftrightarrow \mid T_0, s\rangle$ and $\mid T_\pm, t_0\rangle \leftrightarrow \mid T_0, t_0\rangle$, with the nuclei in $\mid s\rangle$ and $\mid t_0\rangle$ states, respectively, have distinct transition energies and contribute to the central line in the dimer ESR spectrum in Fig. 1(b).

For a given J, the corresponding transition frequencies for the $\mid s\rangle$ and $\mid t_0\rangle$ transition pairs are $\nu_e \pm (\sqrt{J^2 + A^2}/2 - J/2)$[15], and thus they are symmetrically positioned around the center ν_e, split by $\sim A^2/2J$. These transitions are plotted as resonant magnetic fields in Fig. 3(a) (solid blue lines) where for easier comparison with the experimental spectra we show J couplings on a vertical axis and the resonant magnetic fields calculated for each J on a horizontal axis. The symmetric positioning of the resonant fields for all J's implies that after summing over the J distribution as in our samples, the resulting ESR line will be symmetric in contrast to the asymmetric line observed in the experiment (Fig. 1). Therefore, the asymmetric structure must be an effect of the neglected off-diagonal components in the spin-Hamiltonian (Eqn. 2) that mix the singlet and triplet electron and nuclear eigenstates for those dimers having $J \sim \nu_e$.

To verify this effect, we numerically solved the full spin Hamiltonian $\mathcal{H}$, including the off-diagonal terms. The dotted lines in Fig. 3(a) show the positions of the four transitions near the center calculated for different values of the J coupling. As expected, the analytic approximation that gives a symmetric splitting $\sim A^2/2J$ fails for J near $\nu_e = 9.66\,\mathrm{GHz}$. Instead, the off-diagonal terms mix the singlet and triplet electron and nuclear eigenstates for dimers, thus introducing the asymmetric splitting in the resonant fields. Specifically, the triplet state $|T_-, s\rangle$ is mixed with the state $|S, t_-\rangle$ when J is close to ν_e resulting in a doublet transition that is asymmetric about ν_e. To further illustrate this asymmetric splitting, we show in Fig. 3b the CW ESR spectra simulated using the *EasySpin* package[25]. The off-diagonal Hamiltonian terms cause an asymmetric splitting of the transitions about the center, with the largest effect seen when J is close to the Larmor frequency.

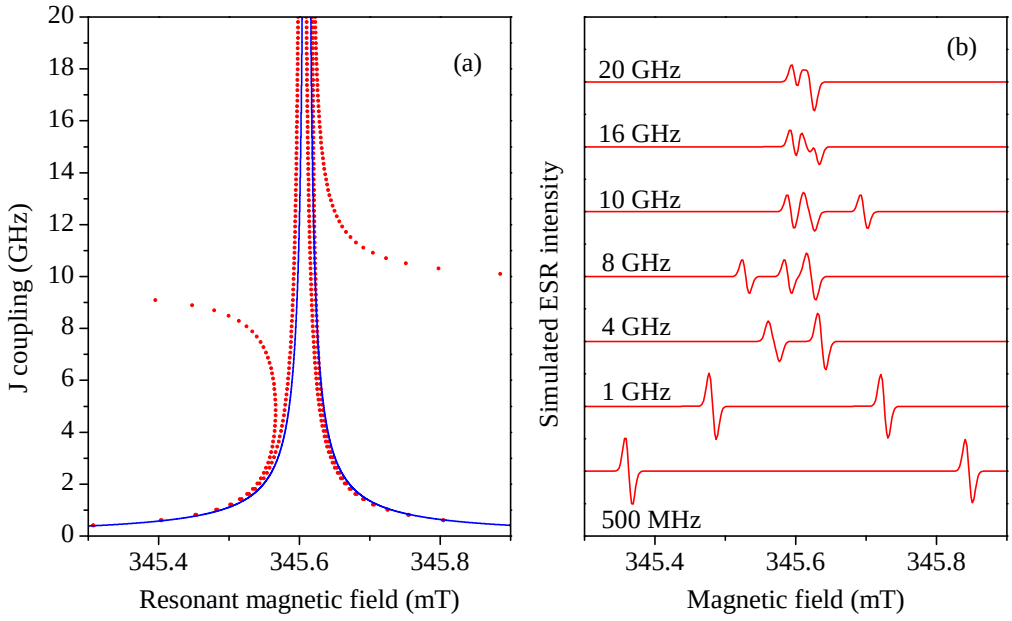

FIG. 3. (a) Resonant magnetic fields for four central ESR transitions in dimers calculated as function of J coupling, assuming the microwave ESR frequency of 9.66 GHz as in experiment. Note that J couplings are shown as a vertical axis and the calculated resonant fields as a horizontal axis. (Solid blue lines) were calculated using the analytical approximation, ignoring the non-diagonal hyperfine terms (Eqn. 2) in the spin Hamiltonian. (Dotted red lines) were calculated numerically, by solving the full spin Hamiltonian $\mathcal{H}$ including the off-diagonal terms. (b) ESR spectra simulated in *EasySpin*[25] for dimers with different J couplings (indicated on each spectrum). These simulations assume a microwave frequency of 9.66 GHz, an inhomogeneous spectral linewidth of 10 µT and a temperature of 15 K. Other simulation parameters are as defined in Eqn. 1.

Since our sample contains dimers with a broad range of J values, the final ESR spectrum comprises a sum of the individual spectra for each J, weighted by the probability distribution of J as shown in Fig. 2. The final simulated CW ESR spectrum is shown in Fig. 4), demonstrating excellent agreement with the experiment in the position of the dimer line and its asymmetric structure. The relative intensity of the low-field sub-structure is somewhat lower in the simulation as compared to the experiment. An extra splitting can also be observed on the high-field line in the simulated spectrum. We ascribe these to the inaccuracy of the estimated J distribution function (Fig. 2). Nevertheless, we can conclude that overall the simulations are in good qualitative agreement, and thus we understand the origin of the

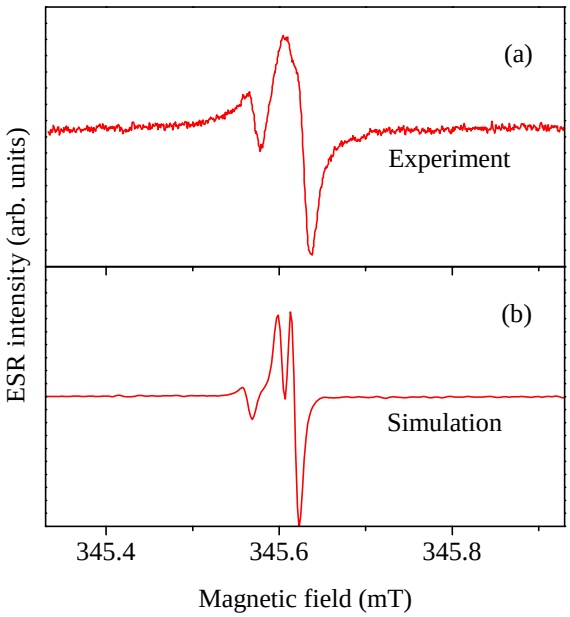

FIG. 4. Comparison of the experimental (a) and simulated (b) CW ESR signals of phosphorus dimers in doped ^{28}Si. The experimental spectrum was measured at 15 K. The simulated spectrum was calculated for $N_d = 2 \times 10^{16}\,\mathrm{cm}^{-3}$, summing the individual spectra over the J distribution function shown in Fig. 2 and assuming $T = 15\,\mathrm{K}$.

fine structure of the phosphorus dimer line in ^{28}Si.

B. T_1 and T_2 of dimers, and comparison to isolated donors

Most of our pulsed ESR measurements were done with the magnetic field centered on the larger high-field structure in the dimer line (referred to as line#1, at 345.63 mT in Fig. 4(a)). The spectral bandwidth in our pulsed experiments was 40 µT, and therefore referring to Fig. 3(a) we infer that dimers with $J > 6\,\mathrm{GHz}$ contributed to the measured relaxation decays, involving all four central transitions, $|\,T_{\pm}, s\rangle \leftrightarrow |\,T_0, s\rangle$ and $|\,T_{\pm}, t_0\rangle \leftrightarrow |\,T_0, t_0\rangle$, with the dimer ^{31}P nuclei in $|\,s\rangle$ and $|\,t_0\rangle$ states. Furthermore, as seen from the probability distribution of J couplings in Fig. 2, 90% of the signal arises from dimers with J less than about 60 GHz.

Fig. 5(a) shows Hahn echo intensity as a function of the total decay time (2τ), at two temperatures. At temperatures between 8 to 4.8 K, the echo decay was distorted after 2 ms decay time into a non-exponential decay, similar to that observed earlier for isolated donors

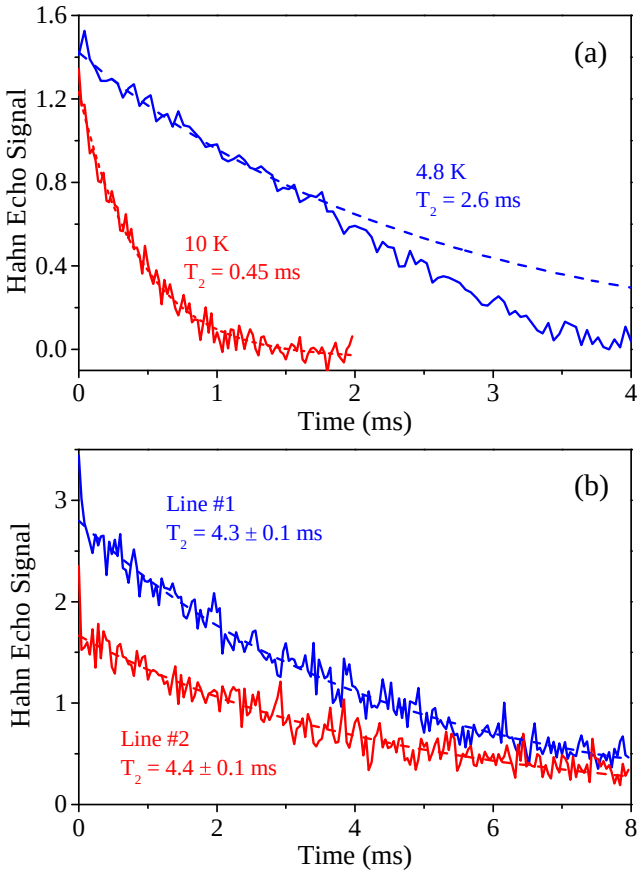

FIG. 5. (a) Hahn echo decays (solid lines) measured by conventional averaging (see text) on the main dimer line at 345.63 mT (a sub-ensemble with 6 GHz $< J <$ 60 GHz) in ^{28}Si at $T = 4.8$ and 10 K, with the respective exponential fits (dashed lines) to extract T_2. Faster than exponential decay after time of 2 ms is an artifact of signal averaging in the presence of echo phase fluctuation due to magnetic field noise[26]. (b) Hahn echo decays (solid lines) with exponential fits (dashed lines), measured at $T = 1.7$ K by magnitude detection (see text). Line#1 (blue) corresponds to the main dimer line at 345.63 mT and line#2 (red) corresponds to the satellite line at 60 μT lower field. The sharp initial drop in the echo signal is an artifact of the destructive interference from partially suppressed ESEEM effects, as discussed further in Sec. III C

in this sample[8]. Such non-exponential decays arise from averaging single-quadrature echo intensities, which fluctuate in phase due to ubiquitous magnetic field noise[26–28]. The distorted decay for times greater than 2 ms was ignored, and only the initial part of the decay was used to extract T_2 for measurements down to 4.8 K.

At $T = 1.7$ K, the spin polarization is large enough that we can measure an echo signal in

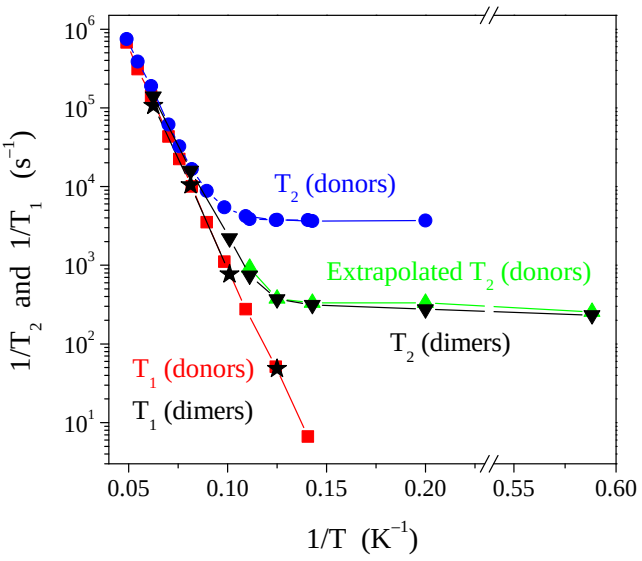

FIG. 6. Temperature dependence of T_1 and T_2 for donors and dimers in ^{28}Si: (stars) dimer T_1, (inverted triangles) dimer T_2, (squares) donor T_1, (circles) donor T_2, and (triangles) donor T_2 after suppressing instantaneous diffusion. The donor T_1 and T_2 data down to 7 K are reproduced from Ref. 8. The lines are guides for eye.

a single-shot, i.e. without averaging. This enables us to average the magnitude of the echo intensity, rather than a single-quadrature, and thus counters the phase fluctuation due to field noise[26]. The echo decay measured by such a magnitude detection technique, shown in Fig. 5(b), displays a simple exponential decay. At 1.7 K, the echo decay was also measured on the low-field satellite line (line #2 at 345.57 mT), where as seen from Fig. 3, only the transition $|T_-, s\rangle \leftrightarrow |T_0, s\rangle$ is excited for dimers with J ranging from 2 to 7 GHz. We find that both dimer sub-ensembles display the same characteristic T_2 of about 4 ms at 1.7 K.

The temperature dependence of T_1 (stars) and T_2 (inverted triangles) for dimers is summarized in Fig. 6 along with the corresponding data for isolated donors (squares and circles), measured in the same ^{28}Si sample. The dimer T_1 is identical to that of donors down to 8 K and is therefore controlled by the same Orbach relaxation mechanism[29] in this temperature range. While we did not measure the dimer T_1 at lower temperatures, we expect it to follow the isolated donor T_1, with $T_1 \sim 1$ hour at 1.25 K[11]. The dimer T_2 follows the T_1 dependence at high temperatures but then saturates at the level of about 4 ms below 8 K. On the other hand, the donor T_2 measured using a standard Hahn echo experiment saturates at an order of magnitude shorter $T_2 = 0.3$ ms. The difference is explained by instantaneous

diffusion[8] that limits the standard Hahn echo T_2 for isolated donors to 0.3 ms in a sample with density of $1.6 \times 10^{16}\,\mathrm{cm}^{-3}$. The effect of instantaneous diffusion was removed as discussed in Sec. II, and the extrapolated T_2 of isolated donors is plotted in Fig. 6 as upright triangles. The extrapolated donor T_2 matches the dimer T_2, saturating at 4 ms. We have recently shown that the donor T_2 at low temperatures (below 8 K) is limited by spectral diffusion due to the dipolar interaction with flip-flopping neighboring donors[19]; it follows from Fig. 6 that the dimer T_2 is limited by the same process.

We note that in the Ref. 19, we showed that the effect of the spectral diffusion process is reduced in samples with lower dopant density, such that the isolated donor T_2 becomes $\sim$ 1 s at 10^{14} cm^{-3}, significantly longer than measured here, though still shorter than the ultimate limit of $2T_1$. It would thus be interesting to measure if the dimer T_2 can also reach 1 s timescales. Such a measurement by an ensemble ESR experiment would however require a differently prepared sample and an improved sensitivity than our current setup.

To conclude, we find no evidence of J coupling causing additional T_1 and T_2 processes between the triplet states, $|\,T_{\pm}, s\rangle \leftrightarrow |\,T_0, s\rangle$ and $|\,T_{\pm}, t_0\rangle \leftrightarrow |\,T_0, t_0\rangle$, in dimers with $6\,\mathrm{GHz} < J < 60\,\mathrm{GHz}$ at temperatures 1.7–20 K. We also found that J-coupling does not limit T_2 for the $|\,T_-, s\rangle \leftrightarrow |\,T_0, s\rangle$ transition in dimers with $2\,\mathrm{GHz} < J < 7\,\mathrm{GHz}$ between 1.7–4.8 K. By measuring the dimer T_2 of 4 ms at 1.7 K and confirming that it is entirely limited by donor flip-flops and thus shows no additional contribution from J-coupling related processes, we can then estimate that T_2 of coherences between the triplet states of isolated dimers should be in excess of 10 ms at low temperatures.

Pulsed ESR experiments probe only transitions between triplet (T_0, $T_{\pm}$) states, and the singlet (S) state remains silent. At first glance, our T_1 and T_2 data as measured for the triplet states do not provide any direct information about dynamics involving the singlet state. However the mixing between the S and T_0 state ($\sim A^2/J$, as shown above) provides a channel for additional decoherence to be observed by ESR[18]. $T_{(S-T0)}$ processes cause irreversible leakage of spin population from triplet states to the singlet state; this leakage (if fast on the time scale of our ESR experiment) will cause a loss of coherence between the triplet states and thus should directly limit the measured T_2. In experiment, we find that $T_2 = 4$ ms at 1.7 K is limited by donor flip-flop processes and thus the $T_{(S-T0)}$ processes contribute insignificantly on this time scale. Therefore, we estimate a lower bound for $T_{(S-T0)}$ to be longer than 10 ms in our sample, for all dimers with $2\,\mathrm{GHz} < J < 60\,\mathrm{GHz}$

at 1.7 K. Our $T_{(S-T0)}$ correlates approximately with $T_{(S-T0)}$ = 1–100 ms as can be derived from theoretical calculations for the one-phonon (direct) relaxation process in donor dimers with J = 2–60 GHz at 1.7 K and magnetic field 0.35 T as in our experiments[18].

C. ESEEM effects in dimer's Hahn echo decays

While measuring dimer's T_2, we observed an unusual dependence of the Hahn echo decays on rotation angles of microwave pulses. Fig. 7(a) illustrates the effect by showing a dramatic change in the echo decay time when using non-selective (broadband) pulses and changing microwave power of the pulses by only 3 dB (corresponds to $\sim 40\%$ change in rotation angles of the pulses). This sharp dependence of the echo decay on a slight change in pulse power is rather unusual and has never been previously reported. Next, we show that this sharp dependence is a result of electron spin echo envelope modulation (ESEEM) arising from the structure of the dimer line.

ESEEM effects in high-spin electron systems ($S > 1/2$) may arise when non-selective microwave pulses excite multiple electron spin transitions[22, 30, 31]. When these transitions have slightly different resonant frequencies, the spin-populations associated with each transition are interconverted by the non-selective refocusing pulse. This gives rise to a modulation of the echo signal decay, with a modulation frequency determined by the difference between the two excited transition frequencies[22].

As discussed above (Sec. III A), several transitions, $|\, T_\pm, s\rangle \leftrightarrow |\, T_0, s\rangle$ and $|\, T_\pm, t_0\rangle \leftrightarrow |\, T_0, t_0\rangle$, from each dimer can contribute to the central dimer line. These transitions are split by $\sim A^2/2J$ (if $|\nu_e - J| \gg A$) which is less than 40 μT for $J > 6$ GHz. This splitting is smaller than the excitation bandwidth of our non-selective pulses, 0.5 mT for pulse lengths of 16 and 32 ns used in experiments shown in Fig. 7(a)). Therefore, all four transitions should be excited by our non-selective pulses, and the resulting echo decay should oscillate with their frequency difference $A^2/2J$. Dimers in our sample are present with a broad range of J and therefore with a broad range of oscillation frequencies. The oscillation frequencies from different J can interfere destructively killing the echo signal at long times. This is exactly what is observed in Fig. 7(a) when using non-selective pulses (blue trace). The situation changes when reducing the power by 3 dB (red trace). Now, the destructive interference is not as effective, leaving the echo signal to decay for long times.

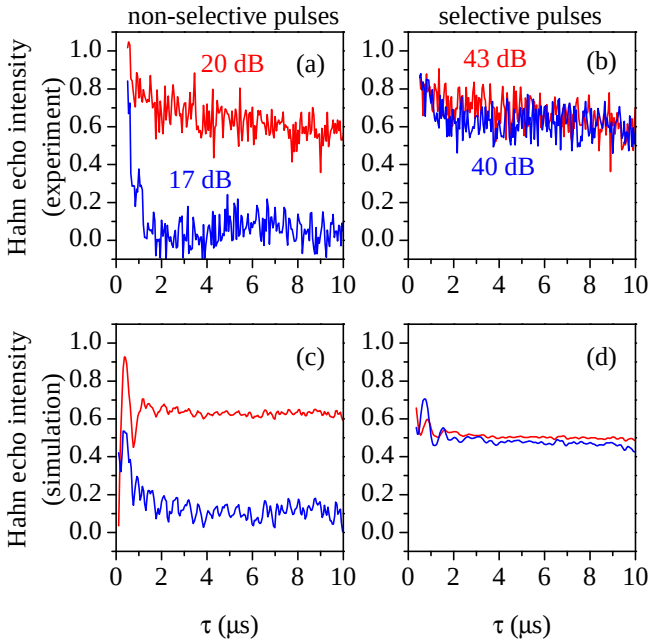

FIG. 7. Hahn echo decays for dimers at two different settings of pulse durations and pulse powers: (a and b) Experimental decays measured using non-selective (16 and 32 ns) and selective (256 and 512 ns) microwave pulses, respectively. Two pulse powers (indicated on each trace as an attenuation level from the maximum output power, 1 kW, of the TWT amplifier) were used in each case. With 16-32 ns (256-512 ns) pulses, the microwave power attenuation level 17 dB (40 dB) was selected so as to produce $\pi/2 - \pi$ rotations for isolated donor spins $S = 1/2$. Measurements were done at 9 K. (c and d) Corresponding simulations using the ESEEM model described in the text.

To verify our ESEEM-related model we repeated Hahn echo experiments using selective microwave pulses (Fig. 7(b)). The excitation B_1 field is set to 35 μT (for 256-512 ns microwave pulses at 40 dB attenuation) that is smaller or comparable to typical dimer splittings. Therefore, only one of the transitions is selectively excited in each dimer (in practice other transitions are still excited but to a lesser extent than the selected transition), and thus the resulting echo decays should show no (or greatly reduced) ESEEM oscillations. The destructive interference should be greatly suppressed, and the echo signal should last for longer times. Indeed, this is what we find in experiment (Fig. 7(b)); both high and low power traces show comparably long decays and no sharp dependence on microwave power is observed as expected.

Before proceeding to numerical simulations of these ESEEM effects, we need to clarify

our choice of microwave powers (B_1 fields) in the experiments shown in Figs. 7(a) and (b). For a spin with $S = 1$ as in our dimers, the choice of optimal power (that at given pulse durations produces $\pi/2 - \pi$ rotations and thus a maximal echo signal) depends on whether pulses are selective or non-selective. In case of non-selective pulses that excite both triplet transitions, $|\, T_+\rangle \leftrightarrow |\, T_0\rangle$ and $|\, T_-\rangle \leftrightarrow |\, T_0\rangle$, the optimal power for the dimer spin ($S = 1$) is the same as for a $S = 1/2$ spin (e.g. isolated donors). On the other hand, in case of selective pulses that excite only one of the triplet transitions, the optimal power should be a factor of 2 smaller (3 dB lower) because the Rabi frequency for $S = 1$ is a factor of $\sqrt{2}$ faster than for $S = 1/2$ (Ref. 23, chapter 6). In our setup, the powers 17 dB (40 dB) for 16-32 ns (256-512 ns) pulses were calibrated such as to produce $\pi/2 - \pi$ rotations (and a maximal echo signal) for isolated donor spins $S = 1/2$. Thus, the power required to achieve $\pi/2 - \pi$ rotations on a dimer selectively or non-selectively were 40 dB or 20 dB, respectively. This calibration procedure allows us to connect the power levels in the experiments with the microwave pulse rotation angle to be used for numerical simulations discussed next.

We numerically simulated the echo signal intensity as a function of τ for dimers with given J, including the magnetic field offset and ESR linewidth as in the experiment. The echo intensity is calculated from the expectation value of S_y traced over the final density matrix $\mathrm{Tr}(U\rho_0 U' S_y)$, where U is the time evolution operator for the pulse sequence and $\rho_0 = S_z$ is the pseudo-pure initial density matrix. $U = U_f U_{p2} U_f U_{p1}$, where U_{p1} and U_{p2} are the evolution operators during the pulses, and U_f is a free evolution operator between the pulses. The free evolution operator is $\exp(-\mathrm{i}2\pi\mathcal{H}\tau)$, where $\mathcal{H}$ is the spin-Hamiltonian of a dimer (Eq. 1), and τ is the delay between pulses. The pulse operators are $\exp(-\mathrm{i}2\pi(\mathcal{H}+\mathcal{H}_{pulse})t_p)$, where $\mathcal{H}_{pulse} = \gamma H_1 S_x$ is the Hamiltonian of the microwave pulse, and t_p is the pulse length. Calculations using the full 16×16 Hamiltonian of a dimer were found to be extremely demanding of CPU power, especially when taking a large number of time steps and averaging over several parameters. Therefore we sped up the calculation by dividing the full 16×16 Hamiltonian matrix $\mathcal{H}$ into four 3×3 matrices (triplet states $S = 1$, one for each out of four nuclear spin states) and four 1×1 matrices (singlet state $S = 0$). We numerically confirmed that the mixing between these matrices is negligible during the spin evolution (less than 0.1%), and therefore each matrix can be evaluated independently. Only two 3×3 matrices need to be evaluated for the 6 dimer eigenstates involved in the central dimer line. The echo signal is calculated by integrating the echo intensity over a window of

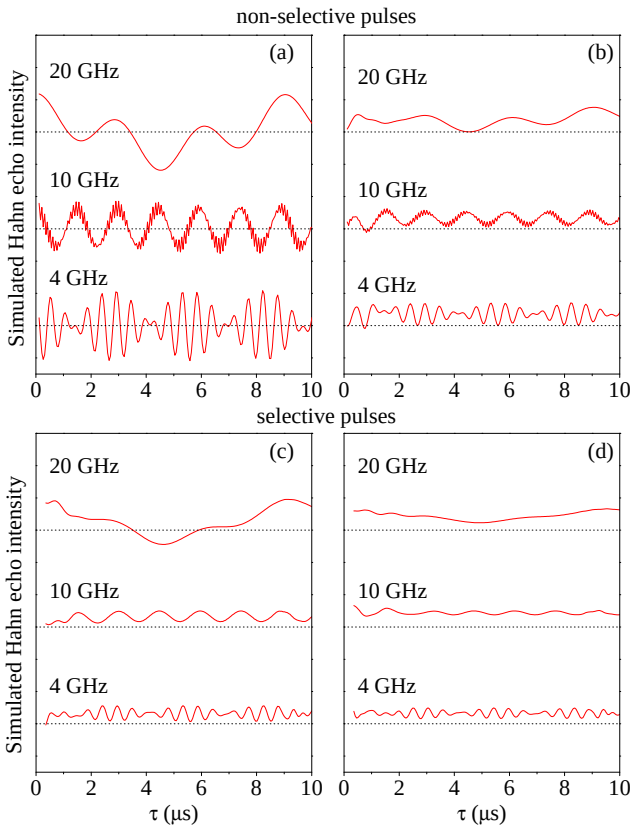

FIG. 8. Simulated Hahn echo signals for different J's assuming a linewidth of 10 μT, a magnetic field centered on the high field line of the dimer spectrum and pulse lengths in (a), (b) of 16-32 ns (non-selective pulses) and in (c), (d) of 256-512 ns (selective pulses). The traces are offset for clarity and the zero line for each trace is marked with dashed lines. In (a), pulse power set so that a 16 ns pulse rotates a donor spin by $\pi/2$. In (c), pulse power set so that a 256 ns pulse rotates a donor spin by $\pi/2$. Pulse power in (b) and (d) are set 3 dB lower than (a) and (c) respectively.

800 ns centered on $2\tau + t_{p1}$, similar to the experiment. The simulated traces were averaged over the inhomogeneous ESR linewidth by including a term $\gamma \Delta H S_z$ in $\mathcal{H}$, where ΔH is an offset magnetic field as seen by a dimer in the ensemble due to inhomogeneity (a Gaussian linewidth of 10 μT was assumed as found in CW ESR simulations).

The representative results of our simulations for J = 4–20 GHz are shown in Fig. 8. ESEEM oscillations are observed in all cases, including non-selective and selective pulses and also large and small pulse rotation angles (pulse powers). The oscillation frequency scales proportionally to $A^2/2J$ as expected. The oscillation amplitude is most pronounced when using non-selective pulses in combination with large rotation angles (Fig. 8(a)). The

oscillations span the full amplitude range, cross zero and invert the signal to negative. The oscillation amplitude is suppressed by a factor of 2 when using smaller rotation angles (Fig. 8(b)). An important improvement with smaller rotations is that the echo traces contain a non-oscillatory (i.e. zero frequency) component. The ESEEM oscillations are further suppressed with selective pulses (Fig. 8(c and d)), as expected because only one of the triplet transitions is selectively excited. Further, the selective pulses at both rotation angles produce a non-oscillatory component in the echo trace.

To calculate the echo signal trace for the dimer ensemble in our silicon crystal we sum up traces like in Fig. 8 over the J coupling distribution shown in Fig. 2. The broad distribution of J couplings implies a broad distribution of ESEEM frequencies. When summed up over this distribution, the oscillating components of the echo signals should average to zero (because of a destructive interference between different frequencies) and only the non-oscillatory components should survive. The summation results are shown in Fig. 7(c and d). The resulting curves qualitatively correlate with the experimental results. In particular, for non-selective pulses and using large rotation angles, the simulated trace decays quickly to zero within the first two microseconds similar to the experiment at 17 dB attenuation. Other traces, including non-selective pulses with small rotation angles and selective pulses at both rotation angles, show a strong signal over a long time range. The residual oscillations seen in all simulated traces are possibly an artifact of averaging over the J distribution (the noise level in the experiment is higher than any of the predicted oscillations). Thus, our simulations confirm that the fast decay of the echo at short τ's in some experiments is an artifact associated with ESEEM that arises from non-selectively exciting both $|\, T_+\rangle \leftrightarrow |\, T_0\rangle$ and $|\, T_0\rangle \leftrightarrow |\, T_-\rangle$ transitions of dimers. To remove this artifact and measure the true dimer T_2 decays requires using selective pulses.

IV. CONCLUSION

We have resolved a new fine structure in the ESR spectra of exchange coupled phosphorus dimers in ^{28}Si. This fine structure had not been observed in previous experiments because of the significant inhomogeneous ESR linewidth caused by the presence of ^{29}Si nuclei in natural silicon samples. We have shown through numerical simulations that this fine structure is a result of singlet-triplet state mixing due to the interplay of the exchange, hyperfine and

Zeeman energies, averaged over the broad J distribution of dimers in doped silicon crystals.

We have also measured the T_1 and T_2 for triplet state transitions of dimers in bulk ^{28}Si. The T_2 experiment is complicated by the presence of ESEEM effects that depend on pulse lengths and powers. By appropriate choice of pulse parameters, we were able to suppress the ESEEM effect and measure the relaxation times. The observed ESEEM effects can be regarded as a spectroscopic signature of J-coupled dimers and can be used in other studies of exchange coupled systems. In ensemble experiments, the ESEEM can show up as artificially fast relaxation decays, while in single dimer studies it might reveal observable modulation effects.

We find that spin coherence times among the triplet states in dimers with $2\,\mathrm{GHz} < J < 60\,\mathrm{GHz}$ at 1.7 K are not affected by the presence of J-coupling at least on time scales up to 10 ms. While we were not able to observe the singlet-to-triplet transitions in dimers directly, we were able to estimate that T_1 leakage from the triplet to singlet state in dimers must be longer than 10 ms, consistent with recent theoretical estimates[18] and experimental results[20]. Note that we are currently unable to put bounds on the decay of coherences between the triplet and singlet state, which is an important topic for further study, since these also limit the fidelity of a two-qubit gate implemented via J-coupling. Furthermore, dimers close to an interface also need to be investigated since they may have shortened coherence, as seen for isolated donors[32].

Appendix: J-coupling distribution for dimers in a silicon crystal with donor concentration of $2 \times 10^{16}\,\mathrm{cm}^{-3}$

Calculations of the J coupling distributions in phosphorus doped silicon crystals have been previously reported in Ref. 15, 33–35. We adapted the previously used methods to calculate the J distribution for the donor density used in our experiments. We use a Monte-Carlo technique by repeatedly and randomly positioning dopants in a given volume. For a donor density N_d, the side of a cube containing on average one donor is $L = 1/N_d^{1/3}$. We simulate a silicon lattice cube of $5L \times 5L \times 5L$ volume which contains on average 125 donors. Since the donors are distributed uniformly, the number of donors in the cube is a Poisson random variable with mean 125. Assuming one of the donors to be at the origin, in each iteration we generate a random number of dopants from a Poisson process with mean 124.

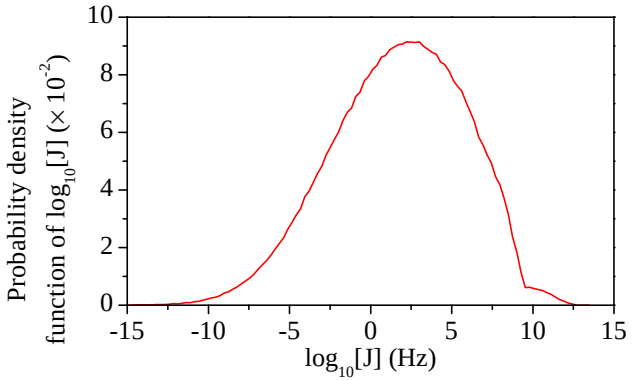

FIG. 9. Probability density function of $\log_{10}[\mathrm{J}]$ for a doping density of $2 \times 10^{16}\,\mathrm{P/cm^3}$ in silicon.

The donors are placed according to a uniform distribution, randomly on the silicon lattice (an FCC lattice with two point basis (000), $a/4(111)$; lattice constant $a = 5.43\,\text{Å}$ [36]).

For each donor configuration, we calculate J couplings between the donor at the origin and all other donors. The expression for exchange coupling, given in the Heitler-London formalism, is taken from Ref. 15. Similar expressions taking into account the oscillatory dependence of J coupling on donor-to-donor distance were also published in Refs. 33 and 37. The donor whose J coupling is maximum is assumed to form a dimer pair with the donor at the origin. In addition, we take into account the possibility of forming trimers and higher order clusters. Thus, we ignore the dimers where the second donor in the pair is more strongly coupled to a third donor. Further, we ignore dimers in which either donor in the pair is coupled to a third donor with a J greater than 1 MHz. The 1 MHz threshold was chosen since a coupling of this strength would result in a dimer ESR signal splitting greater than the ESR linewidth observed in our experiment. On average, for N_d less than $4 \times 10^{16}\,\mathrm{cm^{-3}}$ we found that less than 10 % of a million iterations were ignored, implying that that about 10 % of the donors form trimers or higher order clusters.

The extremely broad range of J values resulting from these calculations is best displayed by calculating the probability density of $\log(J)$. The result is shown in Fig. 9 for a density of $2 \times 10^{16}\,\mathrm{cm^{-3}}$ with J coupling in dimers ranging from 10^{-10} Hz to 10^{13} Hz. The calculated J distribution is in agreement with the results in Ref. 15. Of this broad distribution of J, only the small number of dimers with $J \gg A = 117\,\mathrm{MHz}$ ($\log_{10}(J) > 8$) contribute to the center dimer line in the ESR experiment. The probability density function for these dimers is shown in Fig. 2.

ACKNOWLEDGMENTS

The authors thank Aman Jain, Xuedong Hu and John J. L. Morton for useful discussions. This work was supported by the NSF and EPSRC through the Materials World Network Program (DMR-1107606 and EP/I035536/1) and also by the ARO (W911NF-13-1-0179) and Princeton MRSEC (DMR-01420541).

---

[1] A. Bulanov, G. Devyatych, A. Gusev, P. Sennikov, H.-J. Pohl, H. Riemann, H. Schilling, and P. Becker, Cryst. Res. Technol. **35**, 1023 (2000).

[2] K. M. Itoh, J. Kato, M. Uemura, A. K. Kaliteevskii, O. N. Godisov, G. G. Devyatych, A. D. Bulanov, A. V. Gusev, I. D. Kovalev, P. G. Sennikov, H.-J. Pohl, N. V. Abrosimov, and H. Riemann, Jpn. J. Appl. Phys. **42**, 6248 (2003).

[3] J. W. Ager III, J. W. Beeman, W. L. Hansen, E. E. Haller, I. D. Sharp, C. Liao, A. Yang, M. L. W. Thewalt, and H. Riemann, J. Electrochem. Soc. **152**, G448 (2005).

[4] P. Becker, Metrologia **40**, 366 (2003).

[5] B. E. Kane, Nature **393**, 133 (1998).

[6] M. Cardona and M. L. W. Thewalt, Rev. Mod. Phys. **77**, 1173 (2005).

[7] H. Tezuka, A. R. Stegner, A. M. Tyryshkin, S. Shankar, M. L. W. Thewalt, S. A. Lyon, K. M. Itoh, and M. S. Brandt, Phys. Rev. B **81**, 161203 (2010).

[8] A. M. Tyryshkin, S. A. Lyon, A. V. Astashkin, and A. M. Raitsimring, Phys. Rev. B **68**, 193207 (2003).

[9] J. J. L. Morton, D. R. McCamey, M. A. Eriksson, and S. A. Lyon, Nature **479**, 345 (2011).

[10] F. A. Zwanenburg, A. S. Dzurak, A. Morello, M. Y. Simmons, L. C. L. Hollenberg, G. Klimeck, S. Rogge, S. N. Coppersmith, and M. A. Eriksson, Rev. Mod. Phys. **85**, 961 (2013).

[11] G. Feher, Phys. Rev. **114**, 1219 (1959); G. Feher and E. A. Gere, Phys. Rev. **114**, 1245 (1959); D. K. Wilson and G. Feher, Phys. Rev. **124**, 1068 (1961).

[12] E. Abe, A. M. Tyryshkin, S. Tojo, J. J. L. Morton, W. M. Witzel, A. Fujimoto, J. W. Ager, E. E. Haller, J. Isoya, S. A. Lyon, M. L. W. Thewalt, and K. M. Itoh, Phys. Rev. B **82**, 121201 (2010).

[13] G. Feher, R. Fletcher, and E. Gere, Phys. Rev. **100**, 1784 (1955).

[14] C. Slichter, Phys. Rev. **99**, 479 (1955).

[15] P. Cullis and J. Marko, Phys. Rev. B **1**, 632 (1970).

[16] R. Vrijen, E. Yablonovitch, K. Wang, H. W. Jiang, A. Balandin, V. Roychowdhury, T. Mor, and D. P. DiVincenzo, Phys. Rev. A **62**, 012306 (2000).

[17] D. Culcer, X. Hu, and S. Das Sarma, Applied Physics Letters **95**, 073102 (2009).

[18] M. Borhani and X. Hu, Phys. Rev. B **82**, 241302(R) (2010).

[19] A. M. Tyryshkin, S. Tojo, J. J. L. Morton, H. Riemann, N. V. Abrosimov, P. Becker, H.-J. Pohl, T. Schenkel, M. L. W. Thewalt, K. M. Itoh, and S. A. Lyon, Nat. Mater. **11**, 143 (2012).

[20] J. P. Dehollain, J. T. Muhonen, K. Y. Tan, A. Saraiva, D. N. Jamieson, A. S. Dzurak, and A. Morello, Phys. Rev. Lett. **112**, 236801 (2014).

[21] E. L. Hahn, Phys. Rev. **80**, 580 (1950).

[22] J. J. L. Morton, A. M. Tyryshkin, A. Ardavan, K. Porfyrakis, S. A. Lyon, and G. A. D. Briggs, J. Chem. Phys. **122**, 174504 (2005).

[23] A. Schweiger and G. Jeschke, *Principles of pulse electron paramagnetic resonance* (Oxford University Press, 2001).

[24] J. R. Klauder and P. W. Anderson, Phys. Rev. **125**, 912 (1962); W. B. Mims, Phys. Rev. **168**, 370 (1968).

[25] S. Stoll and A. Schweiger, J. Mag. Res. **178**, 42 (2006).

[26] A. M. Tyryshkin, J. J. L. Morton, S. C. Benjamin, A. Ardavan, G. A. D. Briggs, J. W. Ager, and S. A. Lyon, J. Phys. Cond. Mat. **18**, S783 (2006).

[27] M. J. Biercuk, H. Uys, A. P. VanDevender, N. Shiga, W. M. Itano, and J. J. Bollinger, Nature **458**, 996 (2009).

[28] K. Saeedi, S. Simmons, J. Z. Salvail, P. Dluhy, H. Riemann, N. V. Abrosimov, P. Becker, H.-J. Pohl, J. J. L. Morton, and M. L. W. Thewalt, Science **342**, 830 (2013).

[29] T. G. Castner, Phys. Rev. **155**, 816 (1967).

[30] V. F. Yudanov, K. M. Salikhov, G. M. Zhidomirov, and Y. D. Tsvetkov, Teor. Eksp. Khim. **5**, 663 (1969).

[31] A. D. Milov and Y. D. Tsvetkov, Dokl. Akad. Nauk SSSR **288**, 924 (1986).

[32] T. Schenkel, J. A. Liddle, A. Persaud, A. M. Tyryshkin, S. A. Lyon, R. de Sousa, K. B. Whaley, J. Bokor, J. Shangkuan, and I. Chakarov, Appl. Phys. Lett. **88**, 112101 (2006).

[33] K. Andres, R. Bhatt, P. Goalwin, T. Rice, and R. Walstedt, Phys. Rev. B **24**, 244 (1981).

[34] D. New and T. G. Castner, Phys. Rev. B **29**, 2077 (1984).

[35] D. New, Phys. Rev. B **32**, 2419 (1985).

[36] N. W. Ashcroft and N. D. Mermin, *Solid state physics* (Harcourt, 1976).

[37] B. Koiller, X. Hu, and S. Das Sarma, Phys. Rev. Lett. **88**, 027903 (2001).